INTERNATIONAL JOURNAL FOR NUMERICAL METHODS IN FLUIDS
Int. J. Numer. Meth. Fluids **29**: 921–934 (1999)

MULTIGRID SOLUTIONS OF THE EULER AND NAVIER–STOKES EQUATIONS ON UNSTRUCTURED GRIDS

FANG-PANG LIN*

National Center for High Performance Computing, Hsinchu, Taiwan, Province of China

SUMMARY

A computationally efficient multigrid algorithm for upwind edge-based finite element schemes is developed for the solution of the two-dimensional Euler and Navier–Stokes equations on unstructured triangular grids. The basic smoother is based upon a Galerkin approximation employing an edge-based formulation with the explicit addition of an upwind-type local extremum diminishing (LED) method. An explicit time stepping method is used to advance the solution towards the steady state. Fully unstructured grids are employed to increase the flexibility of the proposed algorithm. A full approximation storage (FAS) algorithm is used as the basic multigrid acceleration procedure. Copyright © 1999 John Wiley & Sons, Ltd.

KEY WORDS: multigrid; edge-based formulation; upwind/LED scheme; FAS algorithm; unstructured meshes

1. INTRODUCTION

The multigrid method was introduced as a solution algorithm for compressible flows in an attempt to enhance the computational efficiency of explicit solution schemes. The importance of the multigrid acceleration technique in this field can be recognized, inspired by the impressive result of Ni [1], who produced solutions of inviscid airfoil flows in the structured grid context. The extension of the technique to incorporate unstructured mesh methods has been successfully developed recently [2,3]. This enables the efficiency of unstructured mesh methods to be considerably improved without loss of the advance features of the unstructured grid approach [4], such as geometrical flexibility and mesh adaptation.

The effectiveness of the multigrid method depends on the following elements: mesh coarsening methods, intergrid interpolation methods and single grid solvers. In the present approach, the advancing front technique [5] is employed to generate a sequence of successively coarser grids, and standard linear and conservative interpolations are used as basic devices for intergrid information transfer. For single grid solvers, unlike most unstructured multigrid procedures that employ multistage time stepping methods with an additional artificial dissipation, an upwind-type scheme is adopted, which allows adaptive control of the numerical dissipation by introducing elaborate non-linear limiting procedures.

The upwind-type scheme can be readily achieved on unstructured grids by using an edge-based data structure [3]. This is accomplished by rewriting the Galerkin approximation of

* Correspondence to: National Center for High Performance Computing, Hsinchu, Taiwan, Province of China.

CCC 0271–2091/99/080921–14$17.50

Received February 1998
Revised April 1998

the equations in an edge-based form (which is locally similar to a one-dimensional form) with special weightings on each edge. In this fashion, monotonicity preserving methods, such as total variational diminishing (TVD) methods [6] and local extremum diminishing (LED) methods [7], can now be extended to multidimensions [8]. LED methods are particularly designed for multidimensional applications and are adopted in the current approach. The steady state flow conditions of interest are computed by advancing the transient form of the equations using an explicit time marching process. The explicit nature of the employed single grid flow solver, and the adoption of LED concepts, make the flow solver less competitive in terms of computational efficiency when compared with classical centered methods. Despite this, it is observed from two-dimensional computational results that the flow solver can be dramatically improved by the multigrid acceleration to compensate this deficiency.

2. THE GOVERNING EQUATIONS

The equations governing 2D compressible flows are considered in a conservation form

$$\frac{\partial \mathbf{U}}{\partial t}+\frac{\partial \mathbf{F}^j}{\partial x^j}-\frac{\partial \mathbf{G}^j}{\partial x^j}=0, \tag{1}$$

where

$$\mathbf{U}=\begin{pmatrix}\rho\\ \rho u^i\\ \rho\epsilon\end{pmatrix}, \qquad \mathbf{F}^j=\begin{pmatrix}\rho u^j\\ \rho u^i u^j-p\delta_{ij}\\ (\rho\epsilon+p)u^j\end{pmatrix}, \qquad \mathbf{G}^j=\frac{1}{Re_\infty}\begin{pmatrix}0\\ \sigma_{ij}\\ \sigma_{ij}u^i-q^j\end{pmatrix} \tag{2}$$

and

$$\sigma_{ij}=2\mu\left(d_{ij}-\frac{1}{3}d_{kk}\delta_{ij}\right), \tag{3}$$

with

$$d_{ij}=\frac{1}{2}\left(\frac{\partial u^i}{\partial x^j}+\frac{\partial u^j}{\partial x^i}\right), \tag{4}$$

$$q^i=-k\frac{\partial T}{\partial x^i}. \tag{5}$$

Here δ_{ij} is the Kronecker delta; ρ, p and ϵ denote the density, pressure and total specific energy of the fluid respectively, and u^j is the component of the fluid velocity in the direction x^j of a Cartesian co-ordinate system. The set of equations is completed by the addition of the perfect gas equation of state

$$p=(\gamma-1)\rho\left(\epsilon-\frac{u^j u^j}{2}\right), \tag{6}$$

where γ is the ratio of the specific heats. The coefficient of viscosity μ varies with the temperature of the fluid and is calculated according to Sutherland's law, and Re_∞ is the Reynolds number based on the airfoil chord.

Steady state solutions are obtained by integrating the governing equations towards stationary conditions. In general, this temporal integral can be regarded as a smoothing process in

iterative schemes. In this manner, numerical schemes used for obtaining the solution of the unsteady governing equations can be viewed as smoothers in the context of the multigrid method. The procedure that will be employed is first developed as a single grid solver and then used as a basic smoother in the multigrid procedure.

3. THE BASIC SMOOTHER

The finite element approach begins with a reformulation of Equation (1) into a variational, or so-called weak form, in which Equation (1) is multiplied by test functions and integrated over the spatial domain. Here, a standard Galerkin approximation, using linear triangular elements, is employed. The detail of the formulation can be found in Reference [4].

3.1. Edge-based formulation

Following Peraire *et al.* [3], after performing the Galerkin approximation, the resulting discrete equations can be constructed by using an edge-based data structure. To derive the equations, it is assume that node I is directly connected by edges to the m_I nodes $I_1, I_2, \ldots, I_{m_I}$ in the grid. Then, the discrete form of the equation at the node I can be written as

$$\left[\mathbf{M}_{\mathrm{L}}\frac{\mathrm{d}\mathbf{U}}{\mathrm{d}t}\right]_I = -\sum_{S=1}^{m_I}\frac{C^j_{II_S}}{2}(\mathbf{F}^{vj}_I + \mathbf{F}^{vj}_{I_S}) + \left\langle \sum_{f=1}^{2} D_f n^j_{II_f}(5\mathbf{F}^{vj}_I + \mathbf{F}^{vj}_{I_f})\right\rangle_I \tag{7}$$

where the first summation extends over all the edges II_S that contain the node I. In the notation employed here, the term $\langle\cdots\rangle_I$ is included only when the node I lies on the computational boundary. In this case, node I is assumed to be common to the boundary faces B_{II_1} and B_{II_2}, where the boundary face B_{II_f} is a boundary edge between two nodes numbered I and I_f. The consistent finite element mass matrix $\mathbf{M}$, which arises from the application of the Galerkin procedure, has been replaced by the standard lumped (diagonal) mass matrix $\mathbf{M}_{\mathrm{L}}$. This allows the construction of truly explicit time stepping procedures and does not alter the final steady state solution, which is of primary concern here. The coefficient $C^j_{II_S}$ denotes the weight, which must be applied to the average value of the flux in the x^j-direction on the edge II_S to obtain the contribution made by this flux and this edge to node I. The form of the coefficients $C^j_{II_S}$ and D_f in Equation (7) are given by

$$C^j_{II_S} = -\sum_{E\in II_S}\frac{2\Omega_E}{3}\left[\frac{\partial N_I}{\partial x^j}\right]_E + \left\langle\frac{\Gamma_f}{6}\boldsymbol{n}^j_{II_S}\right\rangle_{II_S}, \qquad D_f = -\frac{\Gamma_f}{12}. \tag{8}$$

The subscript E represents those edges of elements that are equivalent to the edge II_S and f boundary edges. Ω_E and Γ_f are element area, which contains the edge E, and boundary edge length respectively. $\boldsymbol{n}^j_{II_f}$ and $\boldsymbol{n}^j_{II_S}$ are normal vectors to the edges II_f and II_S. Further details for these coefficients can be found in [3,11]. It is rotationally convenient to normalize the edge coefficients as

$$\mathscr{S}^j_{II_S} = \frac{C^j_{II_S}}{|\boldsymbol{C}_{II_S}|}, \qquad \mathscr{L}_{II_S} = |\boldsymbol{C}_{II_S}|, \tag{9}$$

where the vector $\boldsymbol{C}_{II_S} = (C^1_{II_S}, C^2_{II_S})$. Then, Equation (7) may be expressed in the form

$$\left[\mathbf{M}_{\mathrm{L}}\frac{\mathrm{d}\mathbf{U}}{\mathrm{d}t}\right]_I = -\sum_{S=1}^{m_I}\mathscr{L}_{II_S}\mathscr{F}^{vj}_{II_S}\mathscr{S}^j_{II_S} + \left\langle\sum_{f=1}^{2} D_f\boldsymbol{n}^j_{II_f}(5\mathbf{F}^{vj}_I + \mathbf{F}^{vj}_{I_f})\right\rangle_I, \tag{10}$$

where the edge flux $\mathscr{F}_{II_S}$ is

$$\mathscr{F}_{II_S} = \frac{1}{2}(\mathbf{F}_I^{vj} + \mathbf{F}_{I_S}^{vj})\mathscr{S}_{II_S}^j. \tag{11}$$

3.2. LED extension

To produce a practical algorithm for the flows of interest here, an upwind type multidimensional second-order limited positive ($SLIP_{(2)}$ or $USLIP_{(2)}$) scheme is constructed [7,8]. Following the work of Jameson, the edge flux $\mathscr{F}_{II_S}$ for the $SLIP_{(2)}$ scheme is written as

$$\mathscr{F}_{II_S} = \frac{1}{2}\{(\mathbf{F}_I^{vj} + \mathbf{F}_{I_S}^{vj})\mathscr{S}_{II_S}^j - \hat{\mathbf{R}}_{II_S}|\Lambda_{II_S}|[\Delta \boldsymbol{W}_{II_S} - \mathrm{sign}(\mathscr{A}_{II_S})\min(|\mathscr{A}_{II_S}|, \beta\mathscr{B}_{II_S})]\}, \tag{12}$$

where $\hat{\mathbf{R}}_{II_S}$ denotes the matrix whose columns are the right eigenvectors of the Jacobian matrix $\mathbf{A}_{II_S}$ and $|\Lambda_{II_S}|$ is the absolute value of the diagonal matrix that contains the eigenvalues of $\mathbf{A}_{II_S}$. The hyperbolic nature of the Euler equations allows for the diagonalization

$$|\mathbf{A}_{II_S}| = |\mathbf{A}^j\mathscr{S}_{II_S}^j| = \hat{\mathbf{R}}_{II_S}|\Lambda_{II_S}|\hat{\mathbf{R}}_{II_S}^{-1}. \tag{13}$$

In Equation (12), $\boldsymbol{W}$ is the vector of characteristic variables, β is a positive constant, and $\mathscr{A}$ and $\mathscr{B}$ are respectively defined as

$$\mathscr{A}_{II_S} = (\Delta \boldsymbol{W}_{I_R I} - \Delta \boldsymbol{W}_{II_S} + \Delta \boldsymbol{W}_{I_S I_L}), \tag{14}$$

$$\mathscr{B}_{II_S} = |\mathbf{L}_{II_S}(\Delta \boldsymbol{W}_{I_R I}, \Delta \boldsymbol{W}_{II_S}, \Delta \boldsymbol{W}_{I_S I_L})|, \tag{15}$$

in which $\mathbf{L}_{II_S}$ is a non-linear limiter function and the four node local 1D stencil (I_L, I, I_S, I_R) is constructed by recovering the unknowns at dummy nodes I_L and I_R using a linear interpolation from the nodal values of the triangles in which I_L and I_R lie inside (see Figure 1). The limiter functions can be evaluated in a symmetric or upwind-biased fashion, giving rise to the $SLIP_{(2)}$ and $USLIP_{(2)}$ schemes respectively. The resulting discretized equation, after LED extension, has the form

$$\left[\mathbf{M}_L \frac{\mathrm{d}\mathbf{U}}{\mathrm{d}t}\right]_I = \mathbf{R}_I, \tag{16}$$

where $\mathbf{R}_I$ is the right-hand-side of the discretized form of Equation (10) at node I. This equation can be integrated simply by using an explicit one stage scheme.

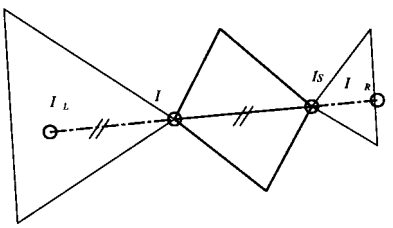

Figure 1. The construction of the TVD scheme on an unstructured grid.

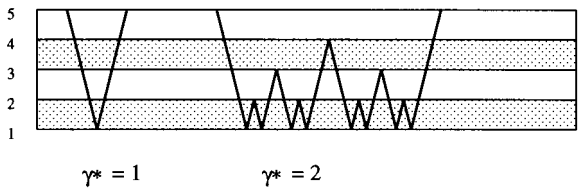

Figure 2. Types of multigrid cycles.

4. MULTIGRID ACCELERATION

The Brandt's full approximation storage (FAS) multigrid algorithm [9] is used. The basic idea of this algorithm is to improve solutions on fine grids by adding corrections, computed from a sequence of successively coarser grids, to the fine grid solutions. The coarse grid equations are solved with the fine grid scheme, but making use of the fact that the allowable time step is larger than that which can be used on the finest grid. The procedure employed here can be readily described using a two grid method. When two grids are used, the fine grid solution $\mathbf{U}_{fI}$ and the corresponding residual $\mathbf{R}_{fI}$, computed as in Equation (11), are transferred onto the coarser grid as $\mathbf{U}_{cI}$ and $\mathbf{R}_{cI}$ and the solution scheme

$$\left[\mathbf{M}_{\mathrm{L}} \frac{\partial \mathbf{U}}{\partial t}\right]_{cI} = \mathbf{R}(\mathbf{U}_{cI}^{n}) - \{\mathbf{R}(\mathbf{U}_{cI}^{0}) - \mathbf{R}(\mathbf{U}_{fI})\}, \quad \forall n \geq 0 \tag{17}$$

is adopted to transport the corrections on this grid. When the coarser grid steps are completed, the corrections are interpolated back to the fine grid and used to update the fine grid solution. Different types of multigrid cycles are defined by γ^*, such that $\gamma^* = 1$ for V-type cycles and $\gamma^* > 1$ for W-type cycles, as illustrated in Figure 2. A sequence of successively coarser grids is obtained by using the advancing front technique. In the advancing front technique, the characteristic of the grid is controlled by the local element spacing δ^i and the local direction α^i of stretching, in which $i \in \{1, 2\}$. By changing the local element spacing from δ^i to $2^k\delta^i$, where the superscript k represents the level of coarsening, coarser grids are then generated [5].

Intergrid information transfer is accomplished by using trivial injection or by performing a conservative interpolation. Both interpolations are illustrated in Figure 3, where an injection for information, e.g. the transfer of $\mathbf{u}$, from the grid B to the grid A can be represented as

$$\mathbf{u}_{I\mathrm{A}} = \sum_{J\mathrm{B}} \mathbf{u}_{J\mathrm{B}} N_{J\mathrm{B}}(x_{I\mathrm{A}}^{j}) \tag{18}$$

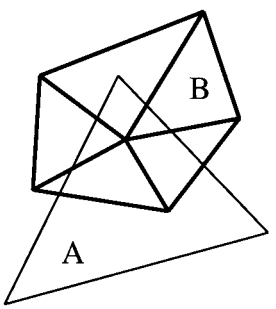

Figure 3. Interpolation between grids.

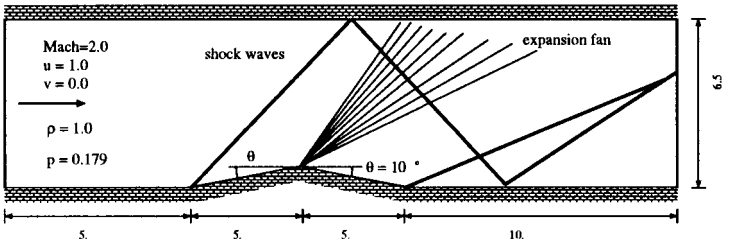

Figure 4. A supersonic inviscid flow at a free-stream Mach number 2.0 over a double 10° wedge in a duct.

and the conservative interpolation can be written as

$$\mathbf{u}_{IA} = [\mathbf{M}_{\mathrm{L}}]_{IA}^{-1} \sum_{IB} [\mathbf{M}]_{IB} \mathbf{u}_{IB} N_{IA}(x^j_{IB}). \tag{19}$$

A further improvement for the conservative interpolation can be achieved by a hybrid interpolation that uses a minmod function over both interpolations [3]. In the application here, injection is used for the transfer of the unknowns from a fine to a coarser grid or for the corrections from a coarse to a finer grid and the hybrid interpolation is used for the transfer of the residuals.

In addition, the second term in the square bracket of Equation (12) can be omitted for the smoothing on coarser grids. This omission avoids the expensive evaluation of the high-order term, which almost doubles the computational CPU time in a sweep, and results in a first-order scheme on coarser grids. In these computations, the employment of the resulting low-order smoother on coarser grids is found to be efficient, in terms of CPU time. A difficulty in achieving convergence of the residual to machine zero may occur due to the non-linear behavior of the limiter $\mathbf{L}_{II_S}$. Here, a limiter freezing technique is adopted to ensure complete convergence. In this procedure, the term $\mathscr{B}_{II_S}$ is fixed as a constant value whenever the residual drops by a pre-defined number of order of magnitude. Further details can be found in [10].

5. MULTIGRID APPLICATIONS

Three examples involving the simulation of supersonic inviscid flows and a subsonic viscous flow are given here to demonstrate the improvement in computational efficiency achieved by using the proposed algorithm. Generally, for the basic smoother, the CFL number is taken to be 0.5, the value of 0.5 is used for β, and a minmod function is adopted for $\mathbf{L}_{II_S}$. For both applications, the results obtained using the multigrid flow solver described here are compared with those obtained using a finite element Taylor–Galerkin and multistage schemes with a second- and fourth-order switched artificial viscosity [10]. It must be remarked that little effort

Figure 5. Density contours with $\rho_{\min} = 0.6303$, $\rho_{\max} = 2.0102$ and an increment interval of 0.02.

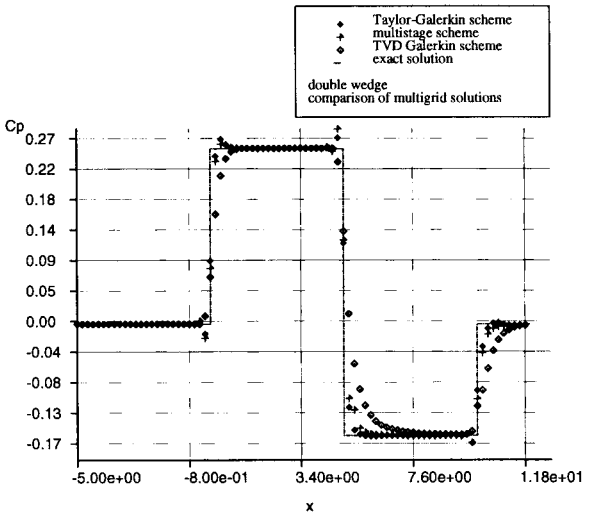

Figure 6. The comparison of the exact and computed C_p on the surface of the double wedge.

was used in order to improve the accuracy of present results. The use of different limiters and stencils for their computation or different choices for the free parameter β are some possibilities to be attempted.

5.1. Flow over a double wedge in a duct

An example of a supersonic inviscid flow at a free-stream Mach number of 2.0 over a double 10° wedge in a duct is considered first. In this case, the flow features, shown schematically in Figure 4, include shocks and an expansion fan. The computation was performed by using a uniform fine grid of 8938 triangular elements and four coarser grids of 2244, 535, 123 and 29 elements. Figure 5 shows the distribution of density contours. The accuracy is examined by

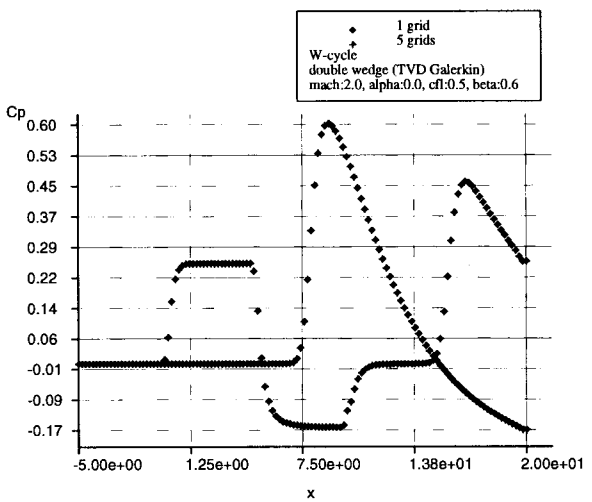

Figure 7. The comparison of C_p along the wall of the double wedge between the single grid method and the multigrid method for the TVD Galerkin scheme.

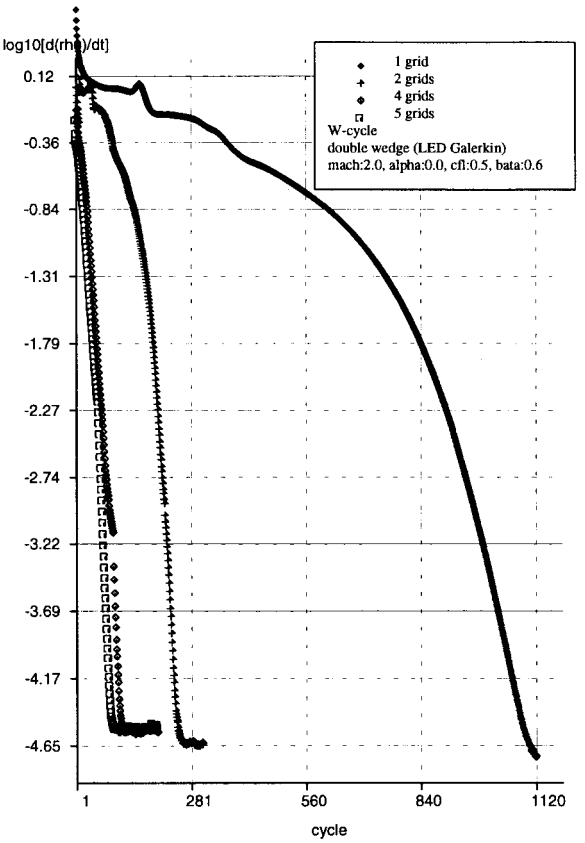

Figure 8. The convergence rates of the W-cycle involving different number of grids.

comparing the computed pressure coefficients along the surface of the double wedge obtained from the other schemes and also from the analytical solution in Figure 6. A W-type cycle is used with one iteration for pre-smoothing on each grid and no post-smoothing applied. The multigrid solutions are compared with the single grid solutions in Figure 7. A pre-conditioning using nested iteration is adopted, in which few cycles, e.g. 20 cycles, are imposed on each level of coarser grids to obtain a better initial guess. The nested iteration begins with smoothing the solutions on the coarsest grid. After some given iterations, the solutions are linearly interpolated to the finer grid. Multigrid cycles are then applied to this fine grid for further solution smoothing. The same smoother is employed on every level of grids. This procedure is repeated until the finest grid is met. The pre-conditioning in practice is equivalent to 8.44 cycles in terms of CPU time. The increase in the rate of convergence towards steady state by the use of the present multigrid scheme is shown in Figure 8, which compares convergence history curves for the flow calculation on the finest grid with those obtained by using the multigrid scheme with various combinations of grids. The CPU time is measured on both the single grid and the multigrid. A ratio of CPU time between one cycle on the mulgrid and one iteration on the single grid is then calculated. The value of this ratio is 3.62 here, which means the CPU time for one multigrid cycle is the same as that for 3.62 single grid iterations. Therefore, considering the CPU time for convergence to machine zero, the multigrid scheme is converged about three times faster than that on the single grid.

5.2. Flow past a cylinder

The second example involves a supersonic flow past a cylinder at a free-stream Mach number of 3.0. Only the front portion of the cylinder is simulated as sketched in Figure 9. Four uniform grids have been considered. These grids, from coarsest to finest, contain 246, 1057, 4320 and 17785 triangular elements respectively. The computed steady state distribution of density contours is shown in Figure 10. A W-type cycle similar to that adopted in the previous example is again employed. Comparison of the distribution of C_p along the surface of the cylinder is shown in Figure 11. A plot showing the convergence history, in terms of the density residual versus number of multigrid cycles, is shown in Figure 12. Similarly, the ratio of the CPU time is measured and its value is 3.68, which results in the multigrid scheme converging two times faster than that on the single grid.

5.3. Viscous flows past NACA0012

The third test case consists of single NACA0012 airfoil at zero degree angle of attack with a free-stream Mach number of 0.5 and a Reynolds number of 5000. An adiabatic wall boundary condition is applied, i.e. the wall boundary is insulated, so that zero heat flux across the airfoil surface is prescribed. The Reynolds number for this case approaches the upper limit for steady laminar flow. For this case, separation occurs near the trailing edge, and a small symmetric recirculation bubble is formed in the trailing-edge and near-wake regions. Three grids are employed. The finest mesh (Figure 13) has 8207 points and 181 points mainly imposed on the surface. The coarsening process is made to ensure that sufficient points remained in the boundary layer in order to have better resolution of the layer even in coarser

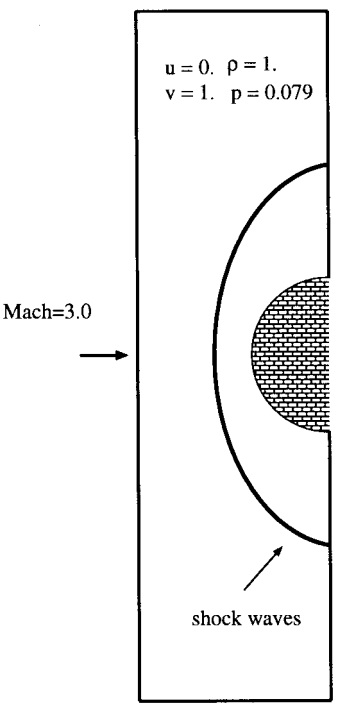

Figure 9. A supersonic inviscid flow passing a cylinder at a free mach number of 3.0.

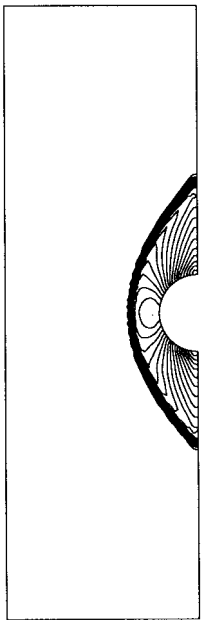

Figure 10. Density contours with $\rho_{\min} = 0.905$, $\rho_{\max} = 4.2688$ and an increment interval of 0.04.

grids. The coarser mesh contains 3271 points with 101 points on the boundaries, and the coarsest mesh contains 1750 points with 86 points on the boundaries. Most of the points are allocated in the boundary layer. The minimum normal spacing at the wall is 0.0002 chords. It is observed that the current method in general gives excessive numerical dissipation at the wall boundary. As a result, the separation point has been shifted towards the downwind direction closer to the trailing edge. A possible way to reduce these excessive terms is to introduce a global parameter to control the whole numerical dissipation. A value of $\frac{1}{2}$ is typically adopted for such a parameter. Smaller values give better results, observed from numerical practice. However, there is a trade-off in efficiency in that, with the reduction of numerical dissipation,

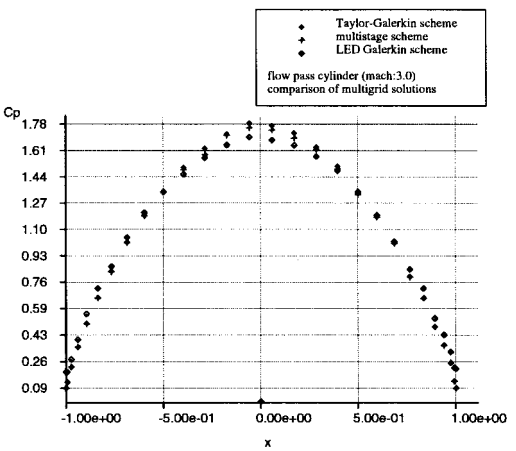

Figure 11. The comparison of the computed C_p along the surface of the cylinder.

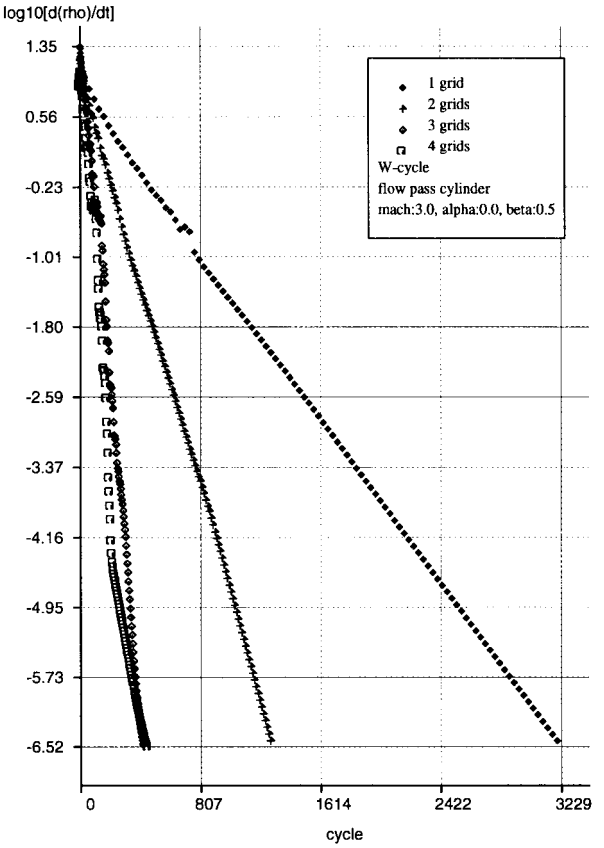

Figure 12. The convergence rates of W-cycle involving different number of grids.

the CFL number has to be reduced correspondingly to ensure the stability of the scheme. This results in the deterioration of the smoothing process and further deteriorates the multigrid performance. An oscillation is also found in the wake region where the boundary mesh is

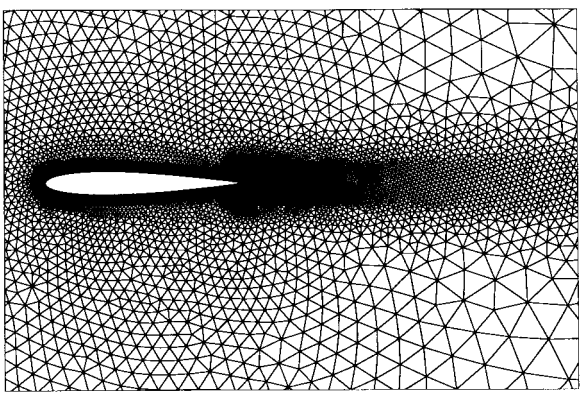

Figure 13. Multigrid for NACA0012 airfoil: finest mesh.

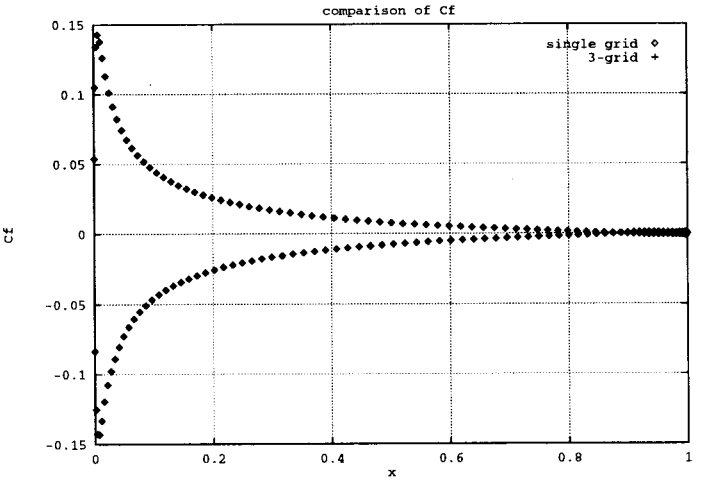

Figure 14. Comparison of the skin friction coefficient.

adapted to the far-field mesh along the trailing edge. A limiter freezing technique for the numerical dissipation has been attempted to suppress this oscillation. The standard W-cycle, i.e. $\gamma^* = 2$, is preferable, according to a previous study for the solutions of inviscid flows. The accuracy must be dominated by the single grid solutions when the multigrid acceleration is incorporated. The numerical solutions are demonstrated in terms of skin friction and pressure coefficients in Figures 14 and 15 respectively. The convergence history is depicted in Figure 16. With the appearance of the boundary layer in the solutions, the convergence rate of multigrid procedure is obviously affected and a deterioration is inevitable. As mentioned previously, the standard method gives excessive numerical dissipation. It is interesting to observe from Figure 16 that the sharpest converged curve is produced by the original method, without an additional tuning parameter for numerical dissipation. The generated spurious dissipation was smoothed efficiently by the multigrid procedure. However, separation never occurs in this case. the

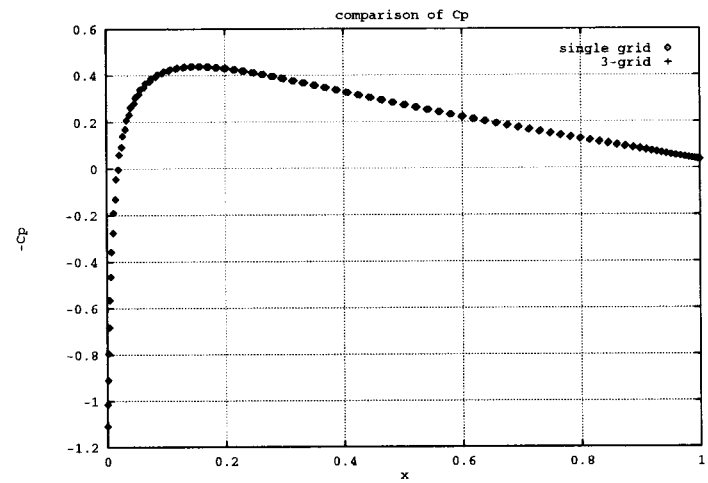

Figure 15. Comparison of the pressure coefficient.

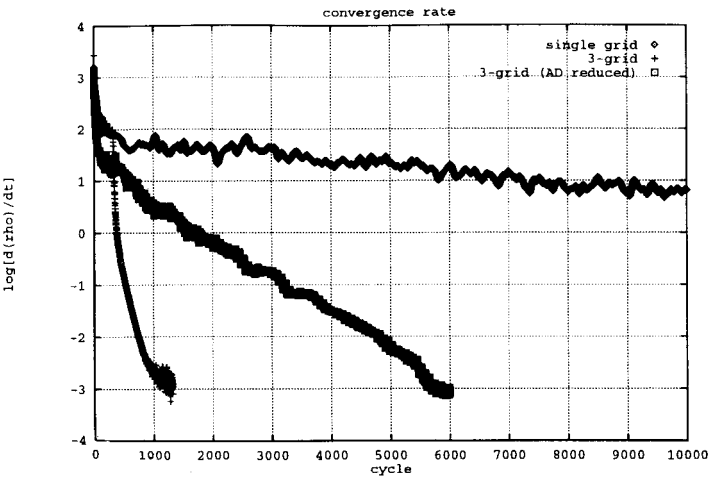

Figure 16. Comparison of convergence rate.

second curve is the standard TVD solver described before, but now the amount of dissipation is reduced by the introduction of a parameter similar to that employed for second-order artificial dissipation in centerd schemes. Good accuracy is achieved. The Courant number used in such circumstances is small, around 0.1 or 0.2. Larger Courant numbers may result in a dissipative solution. Apart from the single grid procedure, the quality of the unrested coarser grids employed here may also contribute to such a deterioration. Enhancement of the coarsening method, e.g. semi-coarsening, may help the convergence towards steady state solutions. The ratio of the CPU time in this case is 3.35. In general, the multigrid procedure demonstrated here has a good performance in comparison with that of the single grid procedure.

6. CONCLUSIONS

It has been demonstrated that an unstructured grid upwind-type scheme can lead to a high accurate shock capturing capability involving the use of a wide variety of limiters with the benefit of geometrical flexibility. Apart from allowing the direct extension of 1D concepts, the adoption of an edge-based data structure provides significant reduction of storage requirements when compared with standard element-based data structure in three dimensions [3]. The low computational efficiency of such schemes, which is caused by the use of low CFL numbers of the explicit method and also the adoption of the LED extension for higher-order accuracy, now has been dramatically improved by the incorporation of the multigrid acceleration procedure as shown in the present encouraging results. A combined procedure, with a high-order scheme on the finest grid and a low-order scheme on coarser grids, is found to be important for better efficiency for the applications attempted here. The use of the LED extension, although improving the robustness of the scheme, produces more diffusive results than those calculated from the reference schemes, the Taylor–Galerkin scheme and the multistage scheme. However, the accuracy of the method can be improved by employing different limiting procedures. The multigrid acceleration procedure crucially improves the practical usefulness of the upwind finite element methods. This suggests that the proposed

algorithm may be well-extended to efficiently solving more challenging problems, such as stationary solutions of high speed viscous flows, and also to incorporating advance mesh adaptivity techniques to acquire generally optimal performance.

ACKNOWLEDGMENTS

The author would like to thank Professor K. Morgan and Dr P. Lyra for their discussions and full supports.

REFERENCES

1. R.H. Ni, 'A multiple grid method for solving the Euler equations', *AIAA Paper 81-1025*, 1981.
2. D.J. Mavriplis, 'Multigrid solution of the two-dimensional Euler equations on unstructured triangular meshes', *AIAA J.*, **26**, 824–831 (1988).
3. J. Peraire, J. Peiró and K. Morgan, 'Finite element multigrid solution of Euler flows past installed aeroengines', *Comput. Mech.*, **11**, 433–451 (1993).
4. K. Morgan, J. Peraire and J. Peiró, 'Unstructured grid methods for compressible flows', *AGARD Report 787 on Special Course on Unstructured Grid Methods for Advection Dominated Flows*, 1992, pp. 5.1–5.39.
5. J. Peraire, M. Vahdati, K. Morgan and O.C. Zienkiewicz, 'Adaptive remeshing for compressible flow computations', *J. Comp. Phys.*, **72**, 449–466 (1987).
6. A. Harten, 'High resolution schemes for hyperbolic conservation laws', *J. Comp. Phys.*, **49**, 357–393 (1983).
7. A. Jameson, 'Artificial diffusion, upwind biasing, limiters and their effect on accuracy and multigrid convergence in transonic and hypersonic flows', *Tech. Report 93-3359*, *AIAA Paper*, 1993.
8. P.R.M. Lyra, 'Unstructured grid adaptive algorithm for fluid dynamics and heat conduction', *Ph.D. Thesis*, University College of Swansea, 1994.
9. A. Brandt, 'Multilevel adaptive solutions to boundary value problems', *Math. Comput.*, **31**, 333–390 (1977).
10. F.P. Lin, 'Multigrid method for compressible flows on unstructured grids', *Ph.D. Thesis*, University College of Swansea, 1995.
11. F.P. Lin, 'Multigrid solution of the Navier–Stokes equations on unstructured grids', *Tech. Report*, *CR/908/96*, University College of Swansea, 1996.

